### Title

Single- and Bi-component T2* analysis of tendon before and during tensile loading, using UTE sequences




### Journal

Journal of Magnetic Resonance Imaging, 42(1)

### ISSN

1053-1807



### Authors

Chang, Eric Y

Du, Jiang

Iwasaki, Kenyu

et al.



### Publication Date

2015-07-01

### DOI

10.1002/jmri.24758

**Original Research**

# Single- and Bi-component T2* Analysis of Tendon Before and During Tensile Loading, Using UTE Sequences

Eric Y. Chang, MD,[1,2]* Jiang Du, PhD,[2] Kenyu Iwasaki, MD, PhD,[2] Reni Biswas, BS,[2] Sheronda Statum, MS,[2] Qun He, PhD,[2] Won C. Bae, PhD,[2] and Christine B. Chung, MD[1,2]

**Background:** To determine if the application of tensile force alters the single- or bi-component T2* values of human tendons as measured on a clinical MRI scanner with ultrashort echo time (UTE sequences and if single- or bi-component T2* values differ when measured with 2D-UTE, 3D-UTE, or 3D-UTE-Cones sequences.

**Methods:** Ten tendons were imaged before and during the application of tension using various UTE sequences at 3 Tesla. Single and bi-component T2* analysis was performed pre- and posttension and compared with Bonferroni-corrected paired Wilcoxon tests.

**Results:** Range of mean pre- and posttension T2* analysis values were: short T2* fraction (78.6–79.7% and 77.3–79.7%, respectively; $P = 1.0$ for all sequences), long T2* fraction (20.3–21.4% and 20.3–22.7%, respectively; $P = 1.0$ for all sequences), short T2* (0.9–1.0 ms and 0.9 ms, respectively; $P = 1.0$ for all sequences), long T2* (19.9–20.4 ms and 21.9–24.0 ms, respectively; $P = 0.9$ for 2D-UTE and $P = 1.0$ for 3D-UTE and 3D-UTE-Cones), and single-component T2* (2.3–2.5 ms and 2.5–3.2 ms, respectively; $P = 1.0$ for all sequences).

**Conclusion:** No significant difference in single- or bi-component results was found after the application of tension to tendons. Results are similar regardless of UTE sequence used for acquisition.

**Key Words:** tendon; tension; ultrashort TE; bi-component analysis
**J. Magn. Reson. Imaging 2015;42:114–120.**


TENDONS TRANSMIT THE force generated by muscles to bone to move the skeleton. The composition of human tendons varies, but those that are subject to primarily tensile stresses such as the Achilles, are composed of approximately 66% water (1) and the dry weight is composed of approximately 87% collagen and 0.2% glycosaminoglycans (2). The ultrastructure of tendon is complex and collagen fibrils not only course in the longitudinal direction, but are also oriented transversely and can form spirals (3). A unique combination of structure and composition confers great strength and a tendon with a cross-section area of 1 $cm^2$ is capable of supporting a weight up to 1000 kg (4).

MRI is a useful method for studying tendons and with the advent of ultrashort echo time (UTE) and similar sequences, signal can be detected in tissues with short mean T2*s (5). With UTE sequences, quantitative MR imaging can be readily performed on tendons. Studies have shown that T2* analysis using single and bi-component analysis may be useful in distinguishing between normal and pathologic tendons (6–8). This has been hypothesized to reflect the known histologic alterations of disruption and disorganization of collagen fibers as well as an increase in total water content (1,9). Specifically, bi-component T2* analysis may reflect the water bound to macromolecules (short component) and free water (long component) in highly organized biological tissues (7,10). Compared with single-component T2* analysis which linearly combines the short and long components, bi-component analysis provides more information which has been shown to be beneficial in evaluating disease states (7).

However, structural and compositional alteration does not only occur in pathologic states. During muscle contraction, tendons are capable of a small amount of elongation (11), which may correspond to straightening of tendon crimps on the microscopic scale (12,13). It is also known from experimental data that tendons under tension decrease their total water content compared with a slack condition (14,15). Despite these changes, statistically significant

[1]Radiology Service, VA San Diego Healthcare System, San Diego, California, USA.
[2]Department of Radiology, University of California, San Diego Medical Center, San Diego, California, USA.
Contract grant sponsor: VA Clinical Science Research and Development Service; Contract grant number: Career Development Grant 1IK2CX000749.
*Address reprint requests to: E.Y.C., VA San Diego Healthcare System, San Diego, CA 92161. E-mail: ericchangmd@gmail.com
Received July 31, 2014; Accepted August 28, 2014.
DOI 10.1002/jmri.24758
View this article online at wileyonlinelibrary.com.

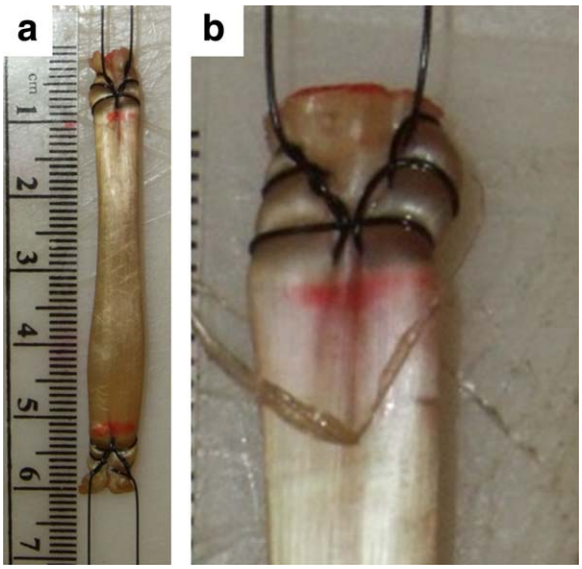


**Figure 1.** Two tendon specimens tied using the Krackow stitch. Flexor digitorum longus (**a**) and magnified peroneus longus (**b**) tendons demonstrate the locking loops which allow the tendon core and periphery to be tensioned and equalized.

differences in transverse relaxation times between tendons under different loading states have not been shown in a previous study (16). However, this previous study used a minimum echo time (TE) of 5 ms and analyzed T2 with single component analysis.

The purpose of this study was to determine if the application of tensile force alters the single- or bi-component T2* values of human tendons as measured on a clinical MRI scanner with UTE sequences and if single- or bi-component T2* values differ when measured with 2D-UTE, 3D-UTE, or 3D-UTE-Cones sequences.

## MATERIALS AND METHODS

### *Sample Preparation*

This anonymized cadaveric study was exempted from the Institutional Review Board. 10 tendon samples were harvested from two donor ankles (2 females, ages 80 and 86 years old), including the tibialis anterior, tibialis posterior, flexor digitorum longus, flexor hallicus longus, and peroneus longus tendons. Specimens underwent a single freeze-thaw cycle, which occurred before dissection.

Tendon samples were cut to a length between 4 and 6 cm. A Krackow stitch (17) was tied to both ends using 2-0 nylon suture (Fig. 1). The Krackow stitch is significantly stronger than simple suture fixation (18) and when both limbs are equalized, the core and periphery of the tendon can be tensioned. Samples were immersed in normal saline for 12 h at 4°C, gently blotted dry, and placed into sealed plastic syringes filled with Fomblin to minimize dehydration and susceptibility artifact (19). Sutures were fixed to one end of the syringe by a red Luer Lock cap and long suture tails were extended out from the opposite plunger end. The rubber stopper maintained the seal

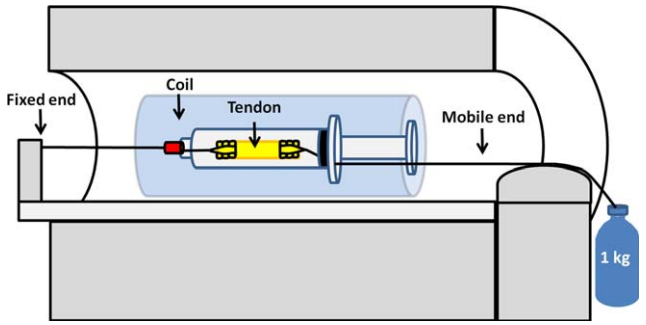


**Figure 2.** Schematic of experimental setup during the application of tension. Tendon is placed inside a syringe and sutures are extended out of the coil with one end fixed to the table and the other, mobile end attached to a suspended water bottle.

and care was taken to ensure tendons were entirely parallel to the long axis of the syringe. At the time of imaging, tendon specimens had been at room temperature for at least 4 h.

### *Tensile Loading and MR Imaging Protocol*

Specimens were placed parallel to the $B_0$ field and imaged in the axial plane on a clinical 3 Tesla (T) MR scanner (Signa HDx, GE Healthcare Technologies, Milwaukee, WI) which had gradients capable of a slew rate of 150 T/m/s and amplitude of 40 mT/m on each axis. Hardware modifications included the addition of a custom transmit–receive switch to the receiver preamplifiers for rapid switching at the end of a radiofrequency excitation pulse to allow ultrashort echo time (UTE) imaging. A wrist coil (BC-10, Medspira, Minneapolis, MN) was used.

For each tendon, one suture end was fixed to the table and the other suture end was extended out of the bore of the magnet. The entire imaging protocol was performed under two conditions, the first with no tensile load applied to the tendon and the second with a 1 liter water bottle (1 kilogram) tied to the mobile suture end at the edge of the table (Fig. 2). A 1 kilogram weight was chosen as a maximum load to fall safely within the tensile strength boundaries of the suture (knotted pull) as rated by the manufacturer (Ethicon, Johnson & Johnson, Cincinnati, OH). The first sequence in the protocol was started 10 min after the load was applied. The majority of tendon lengthening (elastic response) was expected to occur by the time scanning began. However, as other studies have shown (20,21), viscoelastic creep would be expected to continue to elongate our tendon samples to a small degree during scanning. To ensure comparison of similar regions, the midportion of each tendon was used in the analysis (see the Image Analysis section below). A rubber eraser was placed in the field of view of each scan as an external control.

The tendons were imaged in the axial plane with a quantitative imaging protocol consisting of 2D-UTE, 3D-UTE, and 3D-UTE-Cones (22,23) with sequence parameters as shown in Table 1. For each technique, the repetition time (TR) was constant and each

Table 1
Imaging Parameters

| Sequence | TR [ms] | TE [ms] | Flip angle [degrees] | FOV [cm] | Slice thickness [mm] | Matrix | Total imaging Time [min] |
|---|---|---|---|---|---|---|---|
| 2D-UTE | 400 | 0.008, 0.4, 0.8, 1.6, 4.3, 6.0, 8.0, 10.0, 14.0, 16.0, 18.0, 20.0, 24.0, 26.0, 28.0, 30.0 | 60 | 10 | 1.7 | 320x320 | 28 |
| 3D-UTE | 41 | 0.03, 0.4, 0.8, 1.6, 4.3, 6.0, 8.0, 10.0, 14.0, 16.0, 18.0, 20.0, 24.0, 26.0, 28.0, 30.0 | 21 | 10 | 0.4 | 256x256 | 88 |
| 3D UTE-Cones | 40 | 0.03, 0.4, 0.8, 1.6, 4.3, 6.0, 8.0, 10.0, 14.0, 16.0, 18.0, 20.0, 24.0, 26.0, 28.0, 30.0 | 20 | 10 | 1.7 | 320x320 | 60 |

acquisition provided four echoes. In total, 16 echo times (TEs) were acquired ranging from 30 μs to 30 ms to cover the expected T2* values of tendon.

### *Image Analysis*

The images were qualitatively evaluated for the presence of saline-Fomblin fluid levels before and after the application of tension (E.Y.C., 4 years of experience in musculoskeletal radiology). Specifically, a positive fluid level was denoted if saline exuded from the tendon and dependently layered in the Fomblin-filled syringe. All images were reconstructed in multiple planes. The approximate longitudinal tendon lengths before and after tension were recorded on reformatted 3D-UTE images (0.03 ms TE) with electronic calipers because the isotropic voxels would provide the most accurate measurements. The 3D-UTE sequence began approximately 70 min after the onset of tensile loading. Percent change was calculated by: $(L_1–L_0)/L_1$, where $L_0$ represents the pretension length and $L_1$ represents the posttension length on 3D-UTE images.

Using axial images at the midportion of each tendon in the longitudinal axis, regions of interest (ROIs) were carefully placed within the boundaries of the epitenon on the shortest TE image and copied to the corresponding position on subsequent TE images. The mean intensity within each ROI was used for quantitative curve fitting. Single and bi-component T2* analysis was performed using a semiautomated MATLAB (The Mathworks Inc., Natick, MA) code developed in-house as previously described (24,25). In single-component analysis, the UTE signals $S_N(t)$ were fitted with the following equation: $S_N(t) = A \times \exp(-t/T2^*) + \text{noise}$. In bi-component analysis, the UTE signals $S_N(t)$ were fitted with the following commonly used model: $S_N(t) = A_S \times \exp(-TE/T2^*_S) + A_L \times \exp(-TE/T2^*_L) + \text{noise}$, where $A_S$ is the amplitude of the short component, $A_L$ is the amplitude of the long component, $T2^*_S$ is the short component T2*, and $T2^*_L$ is the long component T2*. Apparent short component fraction was defined as $A_S/(A_S + A_L)$. Background noise was estimated using a maximum likelihood estimation distribution fitting of a partial histogram and nonnegative least square curve fitting was used for both single and bi-component models. Fit curves along with their 95% confidence intervals and residual signal curves were created (25). Additionally, single component T2* maps were reconstructed on a pixel-by-pixel basis using various color scales which included all identifiable structures in the field of view, including the tendon, structures attached to the outer surface of the tendon (including paratenon (26) or tendon sheath), and surrounding fluid.

### *Statistical Analysis*

Statistical analyses were performed using the SPSS software package (version 21; SPSS, Chicago, IL). Descriptive statistics were performed for each condition and imaging sequence. The paired Wilcoxon Rank-Sum test was used to compare data before and after the application of tension. Additionally, the paired Wilcoxon Rank-Sum test was used to determine if there were differences between sequences for both the pretension and posttension conditions. Bonferroni correction was performed for multiple comparisons and corrected $P < 0.05$ was considered significant.

## RESULTS

The presence of dependent saline-Fomblin levels in the syringe was noted after the application of tension for each sample (Fig. 3). Each tendon lengthened after the application of tensile load with a mean increase in length of approximately 4.1% (median 3.7%, range 1.4–7.4%).

Curve fitting using the bi-component algorithm was superior compared with the single-component algorithm for all tendons with less than 2% systematic residual signal for each TE for all sequences (Fig. 4). The rubber eraser, included as a reference on all scans, showed mono-exponential decay and demonstrated a single-component T2* value of exactly 0.3 ms on all sequences for both the pretension and posttension conditions ($P = 1.0$), confirming perfect reproducibility. Single component T2* maps showed no appreciable difference between pre- and posttension conditions for each specimen (Fig. 5).

Quantitative results are summarized in Table 2. No significant difference was found for any measurement when compared between the pretension and

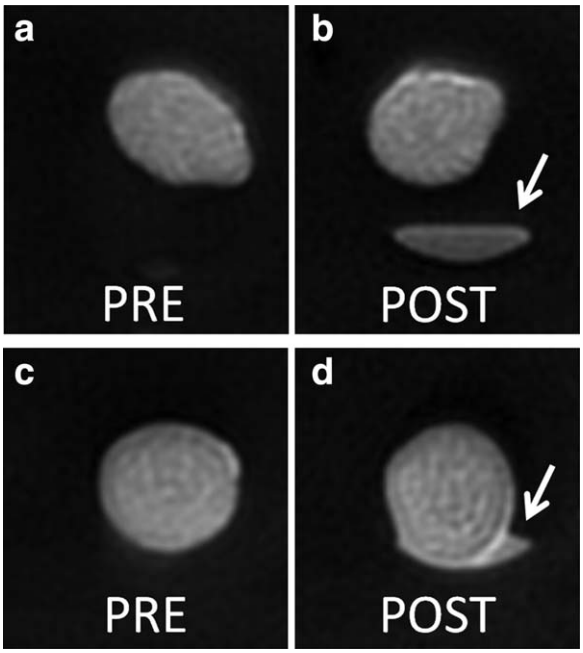


**Figure 3.** Representative 2D-UTE images with 8 μs TE before and after tension. Tibialis anterior **(a,b)** and peroneus longus **(c,d)** tendons show dependent fluid levels (arrows) after the application of 1 kilogram of tensile load.

posttension conditions ($P > 0.05$). Furthermore, no significant difference was found between the 2D-UTE and the 3D-UTE derived measurements, 2D-UTE and 3D-UTE-Cones derived measurements, and 3D-UTE and 3D-UTE-Cones derived measurements for either the pretension (Table 3) or posttension (Table 4) conditions (all $P$ values $> 0.05$).

## DISCUSSION

In this pilot study we imaged tendons before and after the application of tension using various UTE techniques and were unable to find a statistically significant difference between single and bi-component T2* analysis values obtained without and with tension. We were able to visualize the dependent layering of saline which was exuded from the tendon under the loaded conditions, which is consistent with results obtained from prior studies using tendon wet weights (14,15). It is also well known that tendons under load demonstrate loss of crimping and straightening of collagen fibers (13,27–29). The combination of water loss and collagen fiber straightening with tension would have been expected to shorten single-component T2* relaxation times (28) or decrease long T2* bi-component fractions, but was not observed in our samples.

There are a limited number of studies involving MRI measures of tendons under varying static load. However our results are consistent with those by Wellen et al (16), who studied rabbit Achilles tendons under two states of tension including loading with 40 g and 500 g masses. Wellen et al found no significant difference in T2 values between the two loading conditions (16). Of note, Wellen included separate "core" and "rim" measurements and did find nonstatistical trends of T2 differences between the two locations which suggested water transport from tendon core to rim with loading. The regions of interest used in the quantitative portion of our study correspond to the "core" measurements in the study by Wellen et al. We believe that precise segmentation of the outer epitenon rim would be difficult in clinical practice due to surrounding macroscopic fat and other long T2* structures, such as the paratenon and synovial tendon sheaths. Inadvertent inclusion of these structures would confound the results of tendon analysis. However, in our study we did qualitatively evaluate T2* maps which included the "rim" and did not find any discernible difference between loading states.

A secondary objective of our study was to determine the reproducibility of various UTE techniques for the analysis of T2* in tendon. Our study shows that reproducible quantitative measurements can be made

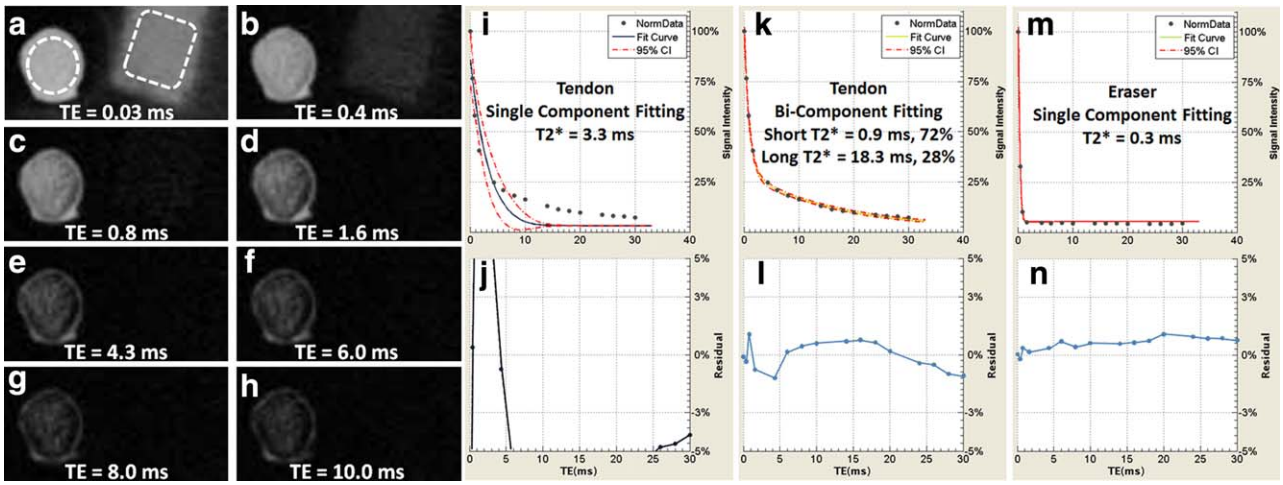


**Figure 4.** 3D-UTE images **(a–h)** showing tendon (circular) and rubber eraser (rectangular) regions of interest. The first 8 TEs are shown for illustrative purposes. Fitting **(i,k,m)** and corresponding residual signal curves **(j,l,n)** show large residual signal using single-component analysis for tendon (I,J) whereas bi-component analysis for tendon (K,L) show minimal residual signal. Rubber eraser (M,N) included for reference shows excellent single-component fit with minimal residual.

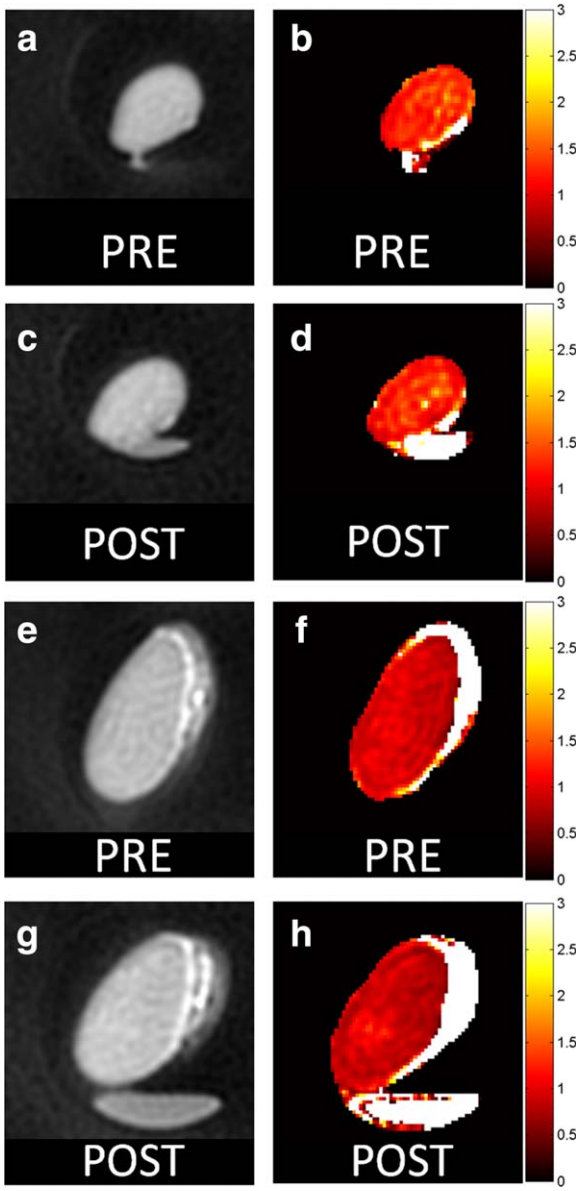


**Figure 5.** Representative 2D-UTE images with 8 μs TE (**a,c,e,g**) and single-component T2* maps (**b,d,f,h**) of two specimens before (A,B,E,F) and after tension (C,D,G,H). Flexor digitorum longus (A–D) and tibialis posterior (E–H) tendons show no appreciable difference in single-component T2* values before and after the application of tension. After the application of tension, dependent fluid levels are visible (C,D,G,H). In addition, both samples contain surrounding long T2* structures such as macroscopic fat and paratenon.

with the 2D-UTE, 3D-UTE, or 3D-UTE-Cones techniques. Our results are similar to some previous studies using UTE techniques with center-out *k*-space acquisitions and single-component (30) and bi-component analysis (10). Other studies have shown slightly different results, including a study by Juras et al who used a variable echo time (*v*TE) sequence with bi-component analysis on in vivo Achilles tendons and found a range of mean values including: 56–62% short fraction, 38–44% long fraction, 0.6–1.0 ms short T2*, and 13.5–23.4 ms long T2* (7). In comparison, range of mean values of our samples was: 77–80% short fraction, 20–23% long fraction, 0.9–1.0 ms short T2*, and 19.9–24.0 ms long T2*. Possible explanations for why our samples showed higher mean short fraction include differences in technique (radial versus Cartesian *k*-space trajectories), differences between living and postmortem tissue, structural and functional differences between tendons, and subject variability.

Zheng and Xia (31) and Wang and Xia (32) have previously highlighted the importance of experimental details for the measurement of multi-component transverse relaxation, including signal-to-noise ratio (SNR), echo spacing, shimming, pulse accuracy, and specimen details. Comparison of the results in this current study with those from two recent studies by Chang et al (19,33), reinforce the important concept that sequence parameters influence bi-component results. With the 2D-UTE parameters used in the previous studies (19,33), bi-component analyses was either unable to be reliably performed or yielded long T2* fractions of less than 5%. In comparison, our current study used the same MRI machine (with the same field strength), specimen orientation, range of echo times, bi-component fitting algorithm, and similar resolution (0.12 $mm^3$ voxel size in the previous studies compared with 0.06–0.27 $mm^3$ voxel size in our current study). Additionally, when we performed retrospective analysis of our data and discarded 4 echoes to approximate the previously used 12 echo times, our bi-component results were unchanged. Other possible explanations for differences in results include differences in SNR, usage of different tendons, or specimen variation. The effect of these and other variables on bi-component quantification using clinical magnets clearly deserves additional study.

Our results should not be compared with other MR measures of tendon under different loading conditions. For instance, Wellen et al (16) found differences in diffusion measurements between tendons under different loading conditions and Helmer et al (34) found differences in proton density. Additionally, recently Syha et al (35) have shown that short-term exercise (consisting of 15 min of high-intensity rope skipping or a cross-country run of 6.6 km) can result in MR-detectable differences in tendons of healthy volunteers using 3D-UTE off-saturation ratio. A decrease in tendon volume was also observed and the combined findings were consistent with a loss of free water molecules within the tendon (35). These results suggest that magnetization transfer techniques may be more sensitive to the short-term water changes in tendon.

Our study has several limitations. First, we included only a small number of samples. As is the nature of pilot studies, our results require external validation with larger sample sizes. Second, tendons can vary widely in structure and function throughout the body (36) and our study results may not be applicable to other tendons such as the Achilles tendon. Third, we did not precondition our tendons or standardize tendon strain despite having a fixed load. Additionally, despite the use of a fixed weight, the force

Table 2
Quantitative Results

| | Pretension | | | | Posttension | | | | |
|---|---|---|---|---|---|---|---|---|---|
| | Mean | Median | Range | SD | Mean | Median | Range | SD | *P*-value* |
| 2D-UTE short T2* fraction (%) | 79.3 | 80.5 | 63.1–88.8 | 8.4 | 79.5 | 80.8 | 65.3–88.8 | 8.6 | 1.0 |
| 3D-UTE short T2* fraction (%) | 79.7 | 81.8 | 66.9–88.9 | 7.3 | 79.7 | 80.5 | 66.1–88.2 | 8.1 | 1.0 |
| 3D-UTE-cones T2* Short fraction (%) | 78.6 | 79.9 | 65.6–88.4 | 7.6 | 77.3 | 77.4 | 63.7–86.0 | 7.9 | 1.0 |
| 2D-UTE long T2* fraction (%) | 20.7 | 19.5 | 11.2–36.9 | 8.4 | 20.5 | 19.2 | 11.2–34.7 | 8.6 | 1.0 |
| 3D-UTE long T2* fraction (%) | 20.3 | 18.2 | 11.1–33.1 | 7.3 | 20.3 | 19.5 | 11.8–33.9 | 8.1 | 1.0 |
| 3D-UTE cones long T2* fraction (%) | 21.4 | 20.2 | 11.6–34.4 | 7.6 | 22.7 | 22.6 | 14.0–36.3 | 7.9 | 1.0 |
| 2D-UTE T2* short (ms) | 1.0 | 0.9 | 0.7–1.8 | 0.3 | 0.9 | 0.8 | 0.7–1.7 | 0.3 | 1.0 |
| 3D-UTE T2* short (ms) | 1.0 | 0.9 | 0.7–1.8 | 0.4 | 0.9 | 0.9 | 0.7–1.8 | 0.3 | 1.0 |
| 3D-UTE-cones T2* short (ms) | 0.9 | 0.8 | 0.6–1.8 | 0.3 | 0.9 | 0.8 | 0.6–1.8 | 0.3 | 1.0 |
| 2D-UTE T2* long (ms) | 20.3 | 19.7 | 13.3–29.8 | 5.3 | 24.0 | 23.8 | 14.8–31.9 | 5.8 | 0.9 |
| 3D-UTE T2* long (ms) | 19.9 | 18.7 | 8.5–30.8 | 6.6 | 21.9 | 21.2 | 15.0–30.5 | 5.2 | 1.0 |
| 3D-UTE-cones T2* long (ms) | 20.4 | 20.1 | 16.5–29.7 | 3.7 | 23.2 | 22.5 | 16.6–33.5 | 5.6 | 1.0 |
| 2D-UTE T2* single component (ms) | 2.4 | 1.9 | 0.9–6.2 | 1.8 | 2.8 | 1.8 | 0.9–9.7 | 2.8 | 1.0 |
| 3D-UTE T2* single component (ms) | 2.3 | 1.6 | 0.9–6.7 | 1.8 | 2.5 | 1.7 | 1.0–7.3 | 2.1 | 1.0 |
| 3D-UTE-cones T2* single component (ms) | 2.5 | 2.1 | 0.8–5.4 | 1.7 | 3.2 | 2.3 | 0.9–10.4 | 3.0 | 1.0 |

*Calculated by paired Wilcoxon Rank-Sum test, Bonferroni corrected *P*-values shown

Table 3
Pretension Sequence Analysis (Bonferroni Corrected *P*-Values)

| | 2D-UTE vs 3D-UTE | 2D-UTE vs 3D-UTE-Cones | 3D-UTE vs 3D-UTE-Cones |
|---|---|---|---|
| Short T2* fraction | 1.0 | 1.0 | 0.9 |
| Long T2* fraction | 1.0 | 1.0 | 0.9 |
| T2* short | 1.0 | 1.0 | 0.15 |
| T2* long | 1.0 | 1.0 | 1.0 |
| T2* single component | 1.0 | 1.0 | 1.0 |

transmitted to the tendon may have been lowered due to friction caused by the suture running between the syringe and plunger. Also, we did not quantify viscoelastic creep which would have caused continuing lengthening of the tendon during the scan protocol. However, to ensure comparable regions, we performed our measurements in the midportion of each tendon (in the longitudinal axis). Fourth, we did not measure the total amount of water in the tendon or water loss with tension. Finally, the imaging time of the sequences used in this study are clearly prohibitively long for clinical translation. However, our protocols were not optimized for time and future studies will be performed to determine how many different TEs and the SNR that is necessary to obtain reliable bi-component analysis results. Additionally, with the use of single slice 2D-UTE or with faster trajectories such as with the use of 3D-UTE-Cones with anisotropic voxels, imaging time can be considerably reduced. The effect of decreased resolution on bi-component analysis also requires additional study.

Table 4
Posttension Sequence Analysis (Bonferroni Corrected *P*-Values)

| | 2D-UTE vs 3D-UTE | 2D-UTE vs 3D-UTE-Cones | 3D-UTE vs 3D-UTE-Cones |
|---|---|---|---|
| Short T2* fraction | 1.0 | 0.15 | 0.15 |
| Long T2* fraction | 1.0 | 0.15 | 0.15 |
| T2* short | 0.15 | 1.0 | 0.15 |
| T2* long | 1.0 | 1.0 | 1.0 |
| T2* single component | 1.0 | 0.3 | 0.3 |

In conclusion, we have found that the application of tensile force did not significantly alter the single- or bi-component T2* values of a small sample of human tendons as measured on a clinical MRI scanner with UTE sequences. Additionally, single and bi-component T2* analysis results are similar regardless of whether a 2D-UTE, 3D-UTE, or 3D-UTE-Cones sequence is used for acquisition.

## REFERENCES


1. de Mos M, van El B, DeGroot J, et al. Achilles tendinosis: changes in biochemical composition and collagen turnover rate. Am J Sports Med 2007;35:1549–1556.
2. Amiel D, Frank C, Harwood F, Fronek J, Akeson W. Tendons and ligaments: a morphological and biochemical comparison. J Orthop Res 1984;1:257–265.
3. Jozsa L, Kannus P, Balint JB, Reffy A. Three-dimensional ultrastructure of human tendons. Acta Anat (Basel) 1991;142:306–312.
4. Maquirriain J. Achilles tendon rupture: avoiding tendon lengthening during surgical repair and rehabilitation. Yale J Biol Med 2011;84:289–300.
5. Chang EY, Du J, Chung CB. UTE imaging in the musculoskeletal system. J Magn Reson Imaging 2014. doi: 10.1002/jmri.24713.
6. Juras V, Zbyn S, Pressl C, et al. Regional variations of T(2)* in healthy and pathologic achilles tendon in vivo at 7 Tesla: preliminary results. Magn Reson Med 2012;68:1607–1613.
7. Juras V, Apprich S, Szomolanyi P, Bieri O, Deligianni X, Trattnig S. Bi-exponential T2 analysis of healthy and diseased Achilles tendons: an in vivo preliminary magnetic resonance study and correlation with clinical score. Eur Radiol 2013;23:2814–2822.
8. Robson MD, Benjamin M, Gishen P, Bydder GM. Magnetic resonance imaging of the Achilles tendon using ultrashort TE (UTE) pulse sequences. Clin Radiol 2004;59:727–735.
9. Jarvinen M, Jozsa L, Kannus P, Jarvinen TL, Kvist M, Leadbetter W. Histopathological findings in chronic tendon disorders. Scand J Med Sci Sports 1997;7:86–95.
10. Du J, Diaz E, Carl M, Bae W, Chung CB, Bydder GM. Ultrashort echo time imaging with bicomponent analysis. Magn Reson Med 2012;67:645–649.
11. Peltonen J, Cronin NJ, Stenroth L, Finni T, Avela J. Viscoelastic properties of the Achilles tendon in vivo. Springerplus 2013;2:212.

12. Hansen KA, Weiss JA, Barton JK. Recruitment of tendon crimp with applied tensile strain. J Biomech Eng 2002;124:72–77.
13. Franchi M, Fini M, Quaranta M, et al. Crimp morphology in relaxed and stretched rat Achilles tendon. J Anat 2007;210:1–7.
14. Nabeshima Y, Grood ES, Sakurai A, Herman JH. Uniaxial tension inhibits tendon collagen degradation by collagenase in vitro. J Orthop Res 1996;14:123–130.
15. Hannafin JA, Arnoczky SP. Effect of cyclic and static tensile loading on water content and solute diffusion in canine flexor tendons: an in vitro study. J Orthop Res 1994;12:350–356.
16. Wellen J, Helmer KG, Grigg P, Sotak CH. Spatial characterization of T1 and T2 relaxation times and the water apparent diffusion coefficient in rabbit Achilles tendon subjected to tensile loading. Magn Reson Med 2005;53:535–544.
17. Krackow KA. The Krackow suture: how, when, and why. Orthopedics 2008;31:931–933.
18. Krackow KA, Thomas SC, Jones LC. Ligament-tendon fixation: analysis of a new stitch and comparison with standard techniques. Orthopedics 1988;11:909–917.
19. Chang EY, Du J, Bae WC, Statum S, Chung CB. Effects of achilles tendon immersion in saline and perfluorochemicals on T2 and T2*. J Magn Reson Imaging 2014;40:496–500.
20. Helmer KG, Nair G, Cannella M, Grigg P. Water movement in tendon in response to a repeated static tensile load using one-dimensional magnetic resonance imaging. J Biomech Eng 2006; 128:733–741.
21. Monleon Pradas M, Diaz Calleja R. Nonlinear viscoelastic behaviour of the flexor tendon of the human hand. J Biomech 1990;23: 773–781.
22. Gurney PT, Hargreaves BA, Nishimura DG. Design and analysis of a practical 3D cones trajectory. Magn Reson Med 2006;55: 575–582.
23. Du J, Bydder M, Takahashi AM, Carl M, Chung CB, Bydder GM. Short T2 contrast with three-dimensional ultrashort echo time imaging. Magn Reson Imaging 2011;29:470–482.
24. Diaz E, Chung CB, Bae WC, et al. Ultrashort echo time spectroscopic imaging (UTESI): an efficient method for quantifying bound and free water. NMR Biomed 2012;25:161–168.
25. Biswas R, Bae W, Diaz E, et al. Ultrashort echo time (UTE) imaging with bi-component analysis: bound and free water evaluation of bovine cortical bone subject to sequential drying. Bone 2012; 50:749–755.
26. Kannus P. Structure of the tendon connective tissue. Scand J Med Sci Sports 2000;10:312–320.
27. Miller KS, Connizzo BK, Feeney E, Tucker JJ, Soslowsky LJ. Examining differences in local collagen fiber crimp frequency throughout mechanical testing in a developmental mouse supraspinatus tendon model. J Biomech Eng 2012;134:041004.
28. Mountain KM, Bjarnason TA, Dunn JF, Matyas JR. The functional microstructure of tendon collagen revealed by high-field MRI. Magn Reson Med 2011;66:520–527.
29. Chang EY, Bydder GM, Statum S, et al. Crimp and macrocrimp behavior in human tendons with ultra-high and high field MRI. In: Proceedings of the 22nd Annual Meeting of ISMRM, Milan, Italy, 2014. (abstract 1179).
30. Gold GE, Pauly JM, Macovski A, Herfkens RJ. MR spectroscopic imaging of collagen: tendons and knee menisci. Magn Reson Med 1995;34:647–654.
31. Zheng S, Xia Y. On the measurement of multi-component T2 relaxation in cartilage by MR spectroscopy and imaging. Magn Reson Imaging 2010;28:537–545.
32. Wang N, Xia Y. Dependencies of multi-component T2 and T1rho relaxation on the anisotropy of collagen fibrils in bovine nasal cartilage. J Magn Reson 2011;212:124–132.
33. Chang EY, Bae WC, Statum S, Du J, Chung CB. Effects of repetitive freeze-thawing cycles on T2 and T2 of the Achilles tendon. Eur J Radiol 2014;83:349–353.
34. Helmer KG, Wellen J, Grigg P, Sotak CH. Measurement of the spatial redistribution of water in rabbit Achilles tendon in response to static tensile loading. J Biomech Eng 2004;126:651–656.
35. Syha R, Springer F, Grozinger G, et al. Short-term exercise-induced changes in hydration state of healthy achilles tendons can be visualized by effects of off-resonant radiofrequency saturation in a three-dimensional ultrashort echo time MRI sequence applied at 3 tesla. J Magn Reson Imaging 2013. doi: 10.1002/jmri.24488.
36. Thorpe CT, Klemt C, Riley GP, Birch HL, Clegg PD, Screen HR. Helical sub-structures in energy-storing tendons provide a possible mechanism for efficient energy storage and return. Acta Biomater 2013;9:7948–7956.